Vacuum 208 (2023) 111701

Contents lists available at ScienceDirect

Vacuum

journal homepage: www.elsevier.com/locate/vacuum

Characterization of a supersonic molecular beam for charged particle beam profile monitor

H.D. Zhang [a,b,*], A. Salehilashkajani [a,b], O. Sedlacek [a,b,c], C.P. Welsch [a,b]

[a] University of Liverpool, Liverpool, L69 7ZX, UK
[b] Cockcroft Institute, Warrington, WA4 4AD, UK
[c] CERN, Geneva, 1211, Switzerland

ARTICLE INFO

Keywords:
Supersonic gas jet
Density measurement
Non-invasive
Beam profile monitor
Supersonic molecular beam

ABSTRACT

In the present work, we report an experimental method to measure the density and distribution of a supersonic molecular beam used for charged particle beam profile monitoring. The density of the molecular beam used in this monitor was in the range of 10^{14}–10^{17} molecules/m^3. The vacuum performance of such a system using beam-induced fluorescence mode was discussed. The successful measurement of the molecular beam parameters paves the way for future applications in beam profile monitors for machines such as the LHC and proton therapy accelerators.

1. Introduction

Noninvasive measurement methods are preferred for modern accelerators to characterize the parameters of the charged particle beams. Ionization profile monitors (IPMs) [1–3] and beam-induced fluorescent monitors (BIFs) [4–8] are widely used as non-invasive beam profile monitors in many accelerators. In such monitors, the particle beams interact with the residual gas, causing the gas molecules to either ionize or emit fluorescent light. The byproducts from the beam–gas interaction can be collected via an external electromagnetic field (ions and electrons) or detected using a stand-alone optical system (fluorescence) to provide the one-dimensional distribution of the primary beams. Depending on the background pressure level, they usually require long integration times or extra working gas being loaded. The latter will create a large pressure bump area and cause a potential degradation of the primary beams. Previous studies [9–13], have shown that the transverse profile of particle beams can be obtained non-invasively by a novel beam profile monitor using a supersonic molecular curtain as a screen. Using a molecular curtain [14] is a novel and safer way to introduce working gases where the molecular beam flows across the charged particle beam in a small and confined area. The signal from the interaction will be significantly increased due to the increased local density but the ambient pressure will be minimally affected due to the directionality of the supersonic molecular beam. Moreover, as shown in Fig. 1, using a curtain beam angled at 45 degrees will have the added benefit of providing a 2D profile of the beams. The thickness, uniformity, and density of the molecular beam curtain screen will affect the accuracy and detection efficiency of such monitors, and thus characterizing these parameters is essential. In addition, supersonic gas jets or molecular beam sources are widely used in high energy physics [15,16], nuclear physics [17,18], nuclear astrophysics [19], and atomic physics [20].

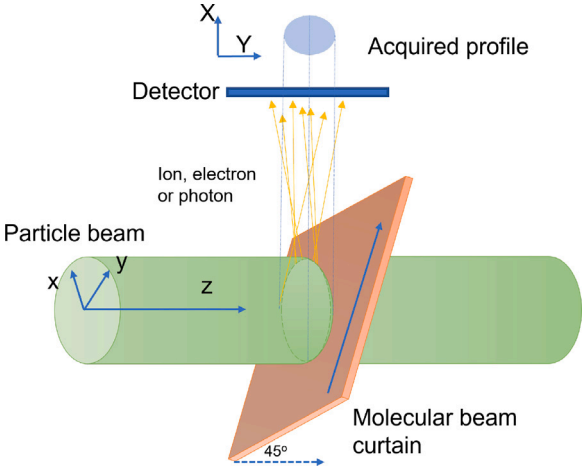

Fig. 1. Concept of using gas jet as a Beam profile monitor.

Previously, the density of gas jets or molecular beam sources was measured overwhelmingly by laser interferometry techniques [21–26]

* Corresponding author at: Cockcroft Institute, Warrington, WA4 4AD, UK.
E-mail address: haozhang@liverpool.ac.uk (H.D. Zhang).

https://doi.org/10.1016/j.vacuum.2022.111701
Received 9 September 2022; Received in revised form 23 November 2022; Accepted 24 November 2022
Available online 28 November 2022

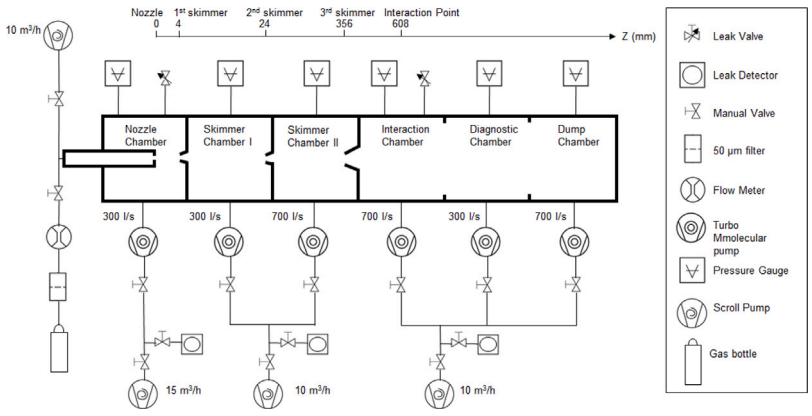

Fig. 2. The layout of the gas curtain beam profile monitor setup, including the vacuum pumping system.

but also by other techniques such as Rayleigh scattering [27], usage of a common microphone [28] or pressure transducer [29], multi-photon ionization [30,31], and nuclear scattering [32]. The target density measured using these methods was in the range of 10^{20}–10^{22} m^{-3}. When dealing with molecular beams with density in the range of 10^{14}–10^{17} m^{-3}, these methods suffer from the signal-to-noise ratio. Compression gauge method [9,10,33] was used to measure the density of a pulsed gas sheet in the range of 10^{16} m^{-3}. We extend this method to measure the absolute density and distribution of a continuous supersonic molecular beam. This enables us to understand the beam profile measured by such monitor and mitigate any distortion due to the thickness and non-uniformity of the gas curtain. The paper is structured as follows. In Section 2, we describe the experimental setup. In Sections 3 and 4, the principle of producing molecular beam curtain and measuring the density using the compression gauge will be explained. In Section 5, the experimental results are presented and discussed together with a comparison from theoretical predication. The conclusions are then summarized in Section 6.

2. Experimental setup

2.1. Supersonic gas curtain monitor system description

The layout with emphasis on pumping details of the setup is shown in Fig. 2 and similar setup were described previously [12,14]. There are three sections including the curtain generation section, interaction section, and gas dump section. The nozzle skimmer assembly separates the curtain generation section into three chambers nozzle chamber, skimmer chamber I, and skimmer chamber II. The supersonic gas jet is generated by injecting high-pressure gas (1–10 bar) from a gas tank through a small nozzle with a diameter of 30 μm into a low-pressure nozzle chamber (10^{-3} mbar). Then the molecular beam is produced by skimming the core of the jet with a conical skimmer with a diameter of 180 μm. It is further collimated by another conical skimmer with a diameter of 400 μm and a pyramid-shaped skimmer with a tip size of 0.4 × 4 mm^2, the molecular beam can travel mono-directionally and be shaped into a screen-like curtain for diagnostic purposes. The differential pumping stages separated by the skimmers were designed to remove the diffused gas molecules and maintain an ultra-high vacuum environment in the interaction chamber. Dumping sections, including the diagnostic chamber and dump chamber, are used for characterizing and dumping the molecular beam. The pressure in each chamber is listed in Table 1 with the stagnation pressure off or continuous on at a stagnation pressure of 5 bar. This clearly shows that the introduction of the molecular beam has a negligible effect on the ultra-high vacuum condition of the interaction chamber.

In the interaction section, the fluorescence induced by the electron beam when interacting with the gas molecules was observed by the

Table 1
Pressure (mbar) in each vacuum chamber, with stagnation pressure off and on at a pressure of 5 bar.

	Nozzle	Skimmer I	Skimmer II	Interaction	Dump
Off	5.0×10^{-8}	5.0×10^{-8}	4.0×10^{-8}	$<1.0\times10^{-9}$	$<1.0\times10^{-9}$
On	3.9×10^{-3}	8.4×10^{-6}	7.3×10^{-7}	4.0×10^{-9}	1.4×10^{-9}

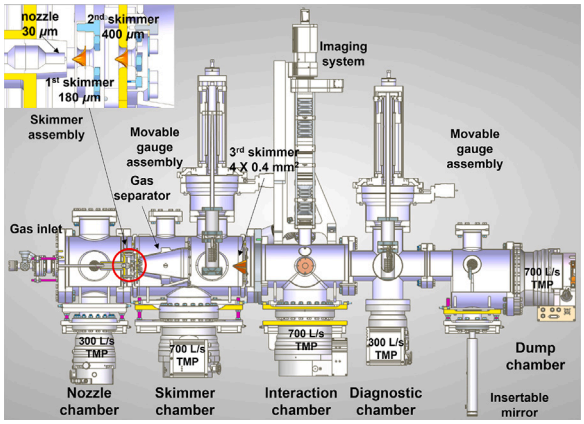

Fig. 3. Schematic drawing of the gas curtain beam profile monitor system.

imaging system including a dedicated band-pass filter with a bandwidth of 10 nm and central wavelength at 391 nm and 585 nm for nitrogen and neon respectively, and an intensified camera system (ProxiKit PKS 2581 TZ-V from ProxiVision GmbH and acA1920-40gm CMOS camera from Basler AG). The schematic drawing of the setup can be seen in Fig. 3. One fluorescence image of a 5 keV and 0.73 mA electron beam obtained by using a nitrogen curtain with a stagnation pressure of 5 bar is shown in Fig. 4 [13]. The fluorescent wavelength is 391.4 nm. The Root Mean Square (RMS) beam size is measured as 0.91 mm and 0.67 mm for x and y, respectively.

2.2. Scanning gauge system

As indicated in Fig. 3, a movable gauge assembly could be installed either between the second and third skimmer or after the interaction chamber. As seen in Figs. 3 and 5, the assembly includes a small chamber consisting of a DN40CF straight connector with the bottom side closed by a fixed flange and the top side attached to a Bayard–Alpert (BA) type ionization gauge. The connector has a length of 125.2 mm, an inner diameter of 34.9 mm, and a wall thickness of 1.55 mm. Two BA gauges were used, one is a series 274 gauge from Granville Phillips Ltd. for the dump section and the other one is an AIG18G gauge from

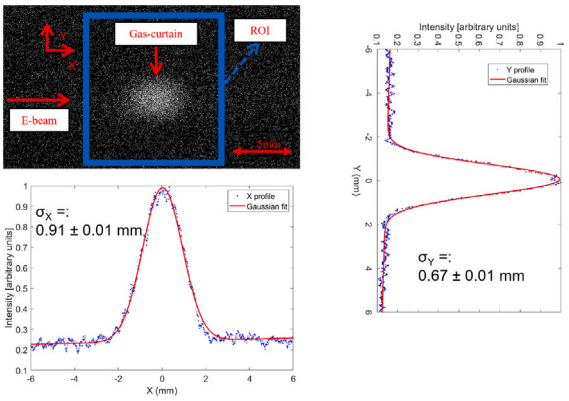

Fig. 4. Image of the nitrogen gas curtain based BIF monitor with an electron beam of 5 keV and 0.73 mA. The integration time is 400 s and the inlet pressure is 5 bar [13].

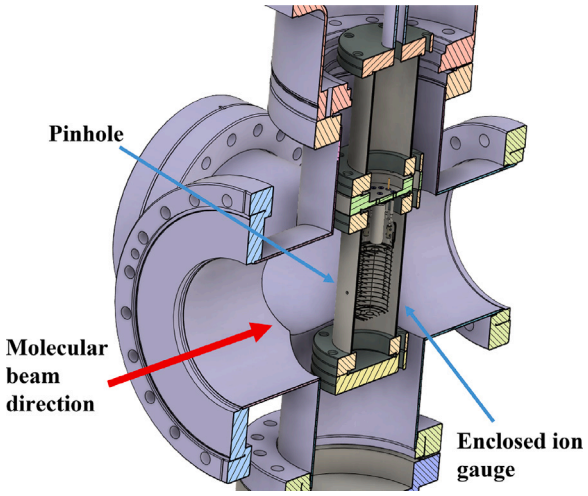

Fig. 5. Schematic drawing of the movable gauge.

Arun Microelectronics Ltd. for the skimmer chamber. The sensitivity factor of nitrogen for both gauges are 7.5 $mbar^{-1}$ and 19 $mbar^{-1}$ respectively. This gauge assembly is then connected to a VACGEN Miniax XYZ manipulator powered by three stepper motors to allow 3-dimensional movement with a minimum resolution of 5 μm. On the tube of the connector, 40 mm above the bottom, there is a pinhole with a diameter of 0.5 mm. The gauge for the dump section is powered by an IGC26 ion gauge controller with an emission current of 0.1 mA by Vacgen Ltd., while the one for the skimmer chamber is powered by an NGC2 ion gauge controller with an emission current of 0.5 mA by Arun microelectronics Ltd. Their signals are amplified by a pico-ampere meter, CP8 by Cooknell Electronics Ltd., and then recorded by an oscilloscope, DS1074 Z-plus by Rigol Ltd.

The ideal position to measure the gas curtain density distribution will be at the interaction point. Due to space limitations, we chose to measure it before and after the interaction point. The geometry of the whole system is summarized as Fig. 6.

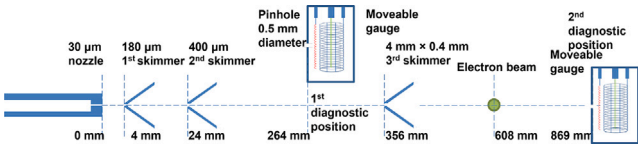

Fig. 6. Schematic of the molecular beam curtain system with two movable gauges.

3. Forming the supersonic molecular beam curtain

As mentioned in Section 2, a supersonic gas jet is generated when a high-pressure gas expands through a 30 μm nozzle into a low-pressure region. From the nozzle to the first skimmer, the center-line density scales as the distance increases, which can be described by Eq. (1) with the assumption of isentropic flow, ideal gas behavior, constant heat capacity, and continuum flow [34].

$$n = \frac{P_0}{k_B T_0}\left(1 + \frac{\gamma - 1}{2} M^2\right)^{-\frac{1}{\gamma - 1}} \tag{1}$$

where γ is the heat capacity ratio, n is the number density, P_0 and T_0 are pressure and temperature at nozzle throat, and M is the Mach number which can be calculated as follow [34]:

$$M = A\left(\frac{x - x_0}{d}\right)^{\gamma - 1} - \frac{\frac{1}{2}\left(\frac{\gamma+1}{\gamma-1}\right)}{A\left(\frac{x - x_0}{d}\right)^{\gamma - 1}} \qquad \left(\frac{x}{d}\right) > \left(\frac{x}{d}\right)_{min} \tag{2}$$

Here x is distance from the nozzle, d is the nozzle throat size, A and x_0 are fitted parameters which are γ-dependent as seen in Table 2. Note that this formula for Mach number [35,36] is a fitting formula for the calculation based on the method of characteristics for an inviscid free-jet flow where the effects of a viscous boundary layer are disregarded.

Table 2
Parameters for center-line Mach number calculation for axisymmetric flow [34].

γ	(x_0/d)	A	$(x/d)_{min}$
1.67	0.075	3.26	2.5
1.40	0.40	3.65	6

The temperature and the velocity of the gas jet in the continuum flow region can be obtained from Eqs. (3) and (4) [34].

$$T = T_0\left(1 + \frac{\gamma - 1}{2} M^2\right)^{-1} \tag{3}$$

$$v_{beam} = \sqrt{\frac{2\gamma}{\gamma - 1}\frac{k_B T_0}{m}} \tag{4}$$

Where T_0 is the temperature of the nozzle, k_B is the Boltzmann constant, and m is the mass of the gas molecule. v_{beam} is the molecule velocity which is assumed to be the terminal velocity since the gas is cooled substantially in the expansion. After the 1st skimmer, the ambient pressure drops below 10^{-5} mbar and the freely-expanding gas jet is skimmed to a molecular beam. The mean free path will be around one meter and thus the collisions between molecules can then be ignored and the gas flow can be regarded as a molecular flow. As a result, geometric expansion can be assumed. The center-line density n of the supersonic molecular beam as a function of the distance from the skimmer L can be calculated from the gas jet parameters at the 1st skimmer using Eqs. (5) and (6)[37].

$$n = n_{skimmer}\left(1 + \frac{L\bar{v}}{r_{skimmer} v_{beam}}\right)^{-2} \tag{5}$$

$$\bar{v} = \sqrt{\frac{3 k_B T_{skimmer}}{m}} \tag{6}$$

Where $n_{skimmer}$ and $T_{skimmer}$ is the center-line number density and temperature of the freely-expanding jet at the location of the 1st skimmer calculated using Eqs. (1) and (3). $r_{skimmer}$ is the radius of the 1st skimmer. $\bar{v}$ is the transverse velocity.

In the calculation, it is assumed an ideal case where the 1st skimmer separates the region of the continuum flow and the molecular flow. The pressure at the nozzle throat is assumed to be the stagnation pressure 5 bar and the temperature at the nozzle throat is 300 K. Then $n_{skimmer}$, $T_{skimmer}$, v_{beam} and $\bar{v}$ can be calculated using Eqs. (1)–(4), (6) as 5.92×10^{20} m^{-3}, 2.3 K, 786.3 m/s and 44.8 m/s for nitrogen and 1.02×10^{21} m^{-3}, 0.12 K, 784.6 m/s and 12.2 m/s for neon. The number density of both gases from the 1st skimmer is calculated using Eq. (5) and the results are shown in Fig. 7. Note that the background scattering and skimmer losses can further reduce the center-line number density, but it is not included in the discussion.

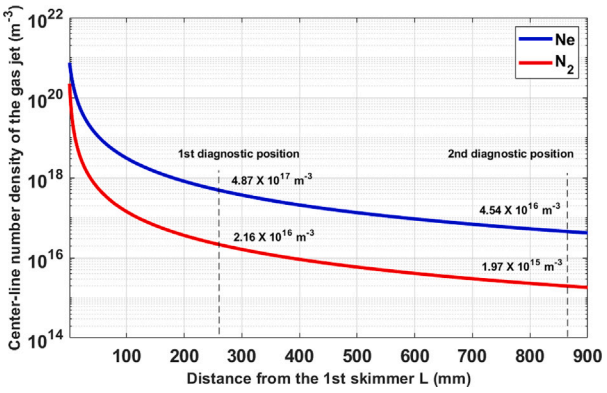

Fig. 7. Calculated center-line number density of the supersonic molecular beam.

4. Measuring principle

The small movable gauge assembly is placed in front of the supersonic molecular beam, as it passes through the system. Part of the beam enters the small chamber through the pinhole and is accumulated inside the small chamber. It results in a higher density and thus a higher ion gauge current reading. The new equilibrium pressure P inside the small chamber is reached when the net effusive flow rate through the hole is equal to the entering rate of the molecular beam. According to [34], this pressure can be expressed as

$$P = \frac{4QIk_BT_1}{\langle v\rangle A} \tag{7}$$

where Q is a factor related to the shape of the pinhole. For the pinhole used in this paper, it is regarded as a round channel with radius r = 0.25 mm and length L = 1.55 mm, Q is calculated as 3.64 according to [38]. $A = \pi r^2$ is the area of the pinhole channel and $\langle v\rangle$ is the mean velocity in the cell at the movable gauge temperature T_1

$$\langle v\rangle = \sqrt{\frac{2k_BT_1}{\pi m}} \tag{8}$$

I is the flux of the molecules entering through the pinhole

$$I = v_{beam}n_{beam}A \tag{9}$$

where v_{beam} and n_{beam} are the longitudinal velocity and the density of the molecular beam, respectively. For the gauge, the increased pressure can be calculated from the difference of the measured ion collector current ΔI_c with or without the molecular beam using Eq. (10).

$$\Delta P = \frac{\Delta I_c}{S_{N_2}R_gI_e} \tag{10}$$

where S_{N_2} is the sensitivity factor for nitrogen, R_g is the gas correction or relative sensitivity factor and I_e is the electron emission current of the chosen gauge. The value for R_g is 1.0 for nitrogen and 0.3 for neon according to the gauge manufacturer. Combining Eqs. (4), (7)–(10), we obtain the density of the molecular beam as

$$n_{beam} = \frac{\Delta I_c}{S_{N_2}R_gI_e}\frac{1}{4Qk_BT_1}\sqrt{\frac{T_1}{T_0}\frac{\gamma-1}{\pi\gamma}} \tag{11}$$

In the analysis, we made several assumptions. First that the molecular beam is uniform and stable on the scale of the pinhole size. Second that the out-gassing rate for the inner surface of the small chamber does not change. Third that at each pinhole location, the new equilibrium inside the small chamber will be established on a time scale of less than one second. These assumptions are reasonable for a continuous molecular beam and a degassed ion gauge. The molecules that enter the small chamber could experience more than 1000 interactions within the chamber surface in one second which is long enough to achieve a new equilibrium.

For the density scan, the manipulator moves the small chamber with the pinhole to a set of coordinates, 0.25 mm per step horizontally and vertically in a region of interest across the molecular beam and beyond. At each coordinate, the collector current of the ion gauge is recorded over 4 s to wait for a new equilibrium to achieve. The current is then averaged and subtracted from the ambient current and the density at that coordinate is calculated from the current difference using Eq. (11). Finally, the density map from all coordinates forms the transverse density map of the molecular beam.

Two error sources were considered, position error and density error. The gauge is mounted on a manipulator, and the resolution and repeatability of the motion in each axis is 5 μm. For the measurement, the step size is always larger than 100 μm, i.e. we can ignore the position error. For a typical B-A type gauge, the measurement error of the current I_c can be 20%. Because of the hot filament of the gauge, the small chamber could be heated up and its temperature T_1 will be slightly higher than the normal room temperature of 300 K. We did not have a direct measurement of that temperature, and instead, a 5% error was used for the temperature. Combining these two errors, one can get a density error of about 20% using Eq. (12).

$$\frac{\sigma_{n_{beam}}}{n_{beam}} = \sqrt{\frac{\sigma^2_{\Delta I_c}}{\Delta I_c^2} + \frac{\sigma^2_{T_1}}{4T_1^2}} \tag{12}$$

where σ is the absolute error for each measurement.

5. Results and discussions

Since the nozzle, 1st and 2nd skimmers are all circular, the ideal transverse distribution of the molecular beam between the 2nd skimmer and the 3rd skimmer is supposed to be rotationally symmetrical. Measurement of such molecular beams with nitrogen and neon as working gases at 1st diagnostic position are shown in Fig. 8. The inlet pressure was 5 bar in both cases and the step size of the movable gauge was 0.25 mm. Both density profiles show a quasi-circular shape. The asymmetry could result from alignment errors related to the nozzle and both skimmers. A Gaussian fit for both dimensions shows a beam size of (0.80 mm, 0.87 mm) for nitrogen and (0.73 mm, 0.81 mm) for neon, respectively. The slightly smaller size of the neon beam is due to the smaller thermal velocity of the neon beam 12.2 m/s as compared to nitrogen 44.8 m/s.

The maximum densities are 2.35×10^{16} m^{-3} for nitrogen molecular beam and 1.20×10^{17} m^{-3} for neon. The differences in density for the two gases depend on the gas molecule status, mono-atomic or diatomic, the molecular weight m, the initial pressure P_0, and temperature T_0. In the continuum flow region, from the nozzle to the first skimmer, the density and the temperature of the molecular beam drop much quicker for a diatomic gas than a mono-atomic gas, so the number density of the nitrogen beam at the skimmer is smaller than the neon beam as shown in Fig. 7. Then in the molecular flow region, the thermal velocity will remain constant when there is no collision. Then the number density reduction is only due to a geometric expansion from this thermal velocity. Comparing this measured maximum number densities to the ones in Fig. 7, one can see that the measured nitrogen beam density is close to the prediction while the neon beam density is ~4 times less. Many factors can contribute to this. First of all, the calculation model for Fig. 7 is too ideal. The transition location from continuum flow to molecular flow can happen before the 1st skimmer. The exact location will decide how much the reduction of number density due to the free expansion will be since the number density decrease monotonically with the distance. In this case, there will be density gain for the start of the geometrical expansion in the molecular flow region if the transition occurs upstream of the 1st skimmer. Moreover, the skimmer loss and background scattering that is not considered will reduce the number density. Second, in the measurement, the misalignment of the nozzle-skimmer assembly will result in a smaller maximum number density which is clearly shown in Fig. 8.

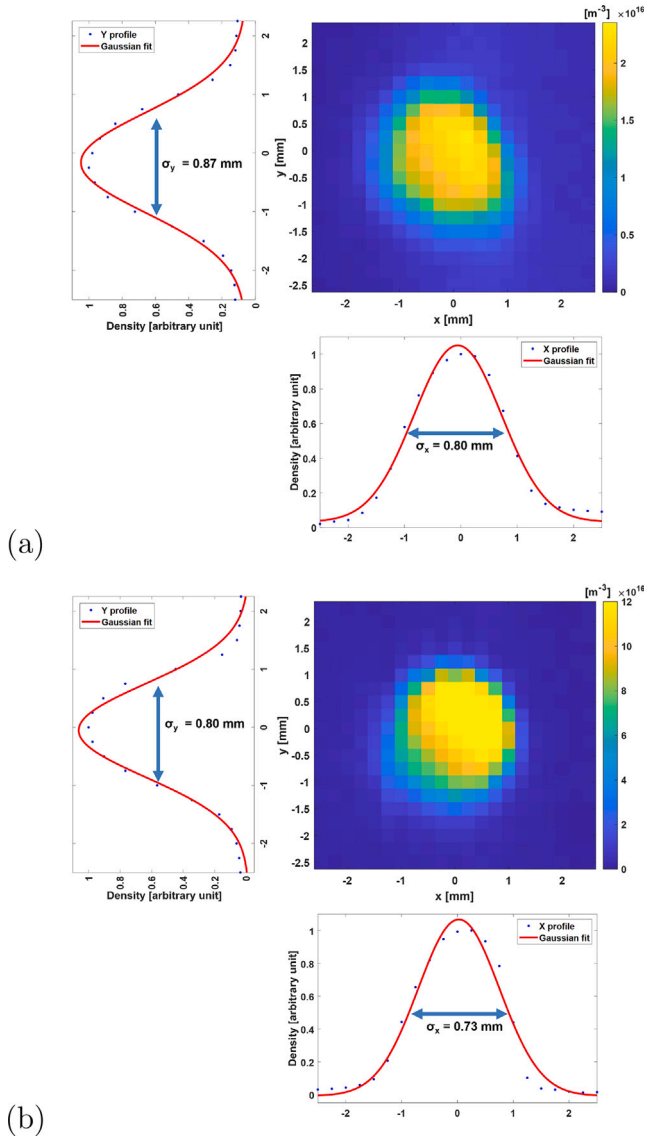

Fig. 8. Measurement of the nitrogen (a) and neon (b) molecular beam density distribution at first diagnostic position.

The density distribution measurement at the 2nd diagnostic position is shown in Fig. 9. The quasi-rectangular shape of the molecular beam is the result of a vertically placed rectangular 3rd skimmer (0.4 mm × 4 mm). Note that the 3rd skimmer is normally placed at a 45-degree angle for beam profile measurement. The full width at half maximum (FWHM) sizes was measured for both cases to be 7.50 ± 0.25 mm (long), 1.25 ± 0.25 mm (short) for nitrogen and 7.63 ± 0.25 mm (long), 1.25 ± 0.25 mm (short) for Neon. The size differences are in the error range which shows there is little difference in the thermal velocity of both molecular beams after they are collimated by the 3rd skimmer. Both distributions show a sharp drop in density at the top and a Gaussian tail at the bottom, which indicates that the 3rd skimmer is off the center compared to the nozzle-skimmer assembly. Similarly, the number density for the neon beam 4.92×10^{15} m^{-3} is still higher than the nitrogen beam 1.40×10^{15} m^{-3} which is consistent with the measurements at the 1st diagnostic position and the geometric expansion assumptions. Again, the maximum number density of the nitrogen beam is close to the calculated center-line number density at the 2nd diagnostic position while for the neon beam, it is much smaller. Note that a measurement range from 10^{14} to 10^{17} m^{-3} can be summarized from both Figs. 8 and 9.

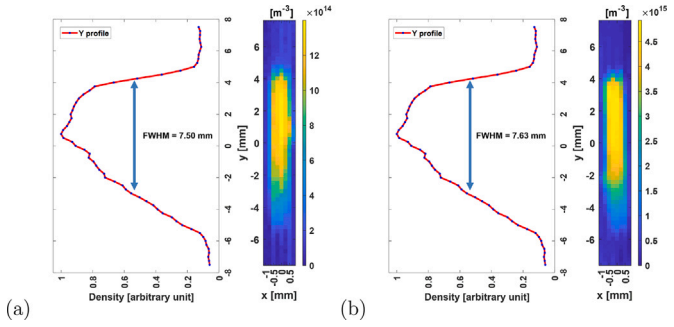

Fig. 9. Measurement of the nitrogen (a) and neon (b) molecular beam density distribution at the second diagnostic position.

Due to the finite size of the pinhole for the movable gauge, the distribution measured here will be a convolution of the real number density distribution with the pinhole size. To retrieve the real distribution, a deconvolution method was used. Since the distribution for a highly collimated molecular beam tends to be uniform, a uniform beam with sizes a (long) and b (short) is assumed to be the real distribution. Then it becomes an optimization problem to find the sizes a and b when the cost function between the convolution of the uniform distribution with these sizes and the measured distribution is minimized. In practice, the genetic algorithm was used for the deconvolution process and it gives the sizes as 8.32 mm (long), 0.96 mm (short) for nitrogen and 7.54 mm (long), 0.87 mm (short) for neon. The convoluted density distribution of the uniform beam with these parameters is shown in Fig. 10, which shows a good match with the measurements in Fig. 9. Note that the de-convolution will be more effective with the scanning steps smaller than 0.25 mm. The reason why this step was used is a trade-off between experiment time and accuracy. Theoretically, the scanning steps can be as small as 5 μm as previously mentioned.

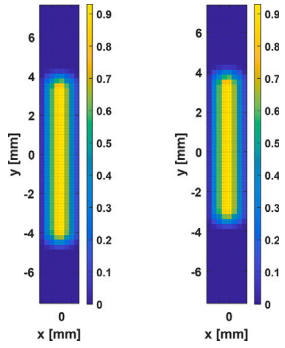

Fig. 10. Convoluted images of uniform molecular beam distributions with the pinhole matched with the measurement: left: Nitrogen; right: Neon.

For beam profile measurements, the vertical size of the molecular beam curtain defines the range one can use to characterize the primary beam. The thickness and the uniformity of the molecular beam curtain will determine the smearing effects and hence the image quality. From our jet density measurement, both measurements show a good uniformity in the central area in the 2nd diagnostics position. From the 3rd skimmer to the interaction point and then the 2nd diagnostics position, the gas flow is a molecular flow where no collision will occur. Thus, for the interaction point, the gas curtain thickness can be estimated by a linear expansion from 0.4 mm at the 3rd skimmer location to 1.25 mm at the 2nd diagnostic position as shown in Fig. 11, which gives a thickness of 0.85 ± 0.14 mm at the interaction point.

6. Conclusion

In this paper, we described a method to measure the absolute density and the density distribution of a supersonic molecular beam in

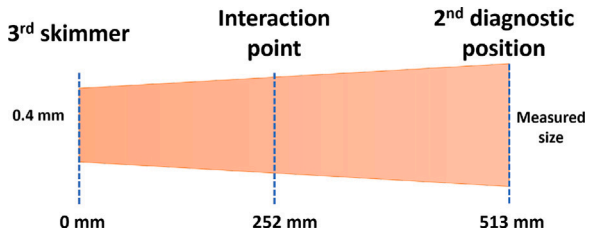

Fig. 11. Estimate the curtain sizes in the interaction point by a linear expansion from the 3rd skimmer.

the molecular flow region. This method was applied to a supersonic gas curtain used for charged particle beam profile monitors. It is capable to measure the number density of both nitrogen beam and neon beam in the range from 10^{14} to 10^{17} m^{-3} with a good spatial resolution of sub-mm. The spatial resolution is limited by the pinhole size but can be reconstructed by the de-convolution method if a known distribution (uniform distribution here) is assumed. The measurement of the molecular beam density and its distribution will allow a further study or optimization of the gas curtain by changing the geometry of the skimmers to meet different diagnostics requirements such as charged particle beam intensity, integration time, and ambient vacuum environment. Currently, this method is used regularly for characterizing a supersonic gas curtain in the beam profile monitor [39] designed for the LHC proton beam where a uniform gas curtain with 1×10^{16} to 1×10^{17} m^{-3} density and 0.5 mm thickness is required to achieve an integration time of 1 s. This method could also be applied to similar supersonic molecular beams used in other fields such as nuclear targets and atomic physics. The recent development of a beam profile and dose monitor for medically used charged particle beam [40] is another example where the measurement of the gas curtain density and its distribution will help in the designing and commissioning phases.

CRediT authorship contribution statement

H.D. Zhang: Writing – review & editing, Writing – original draft, Visualization, Validation, Supervision, Software, Resources, Project administration, Methodology, Investigation, Formal analysis, Data curation, Conceptualization. **A. Salehilashkajani:** Writing – review & editing, Writing – original draft, Visualization, Data curation. **O. Sedlacek:** Writing – review & editing, Visualization, Software. **C.P. Welsch:** Writing – review & editing, Supervision, Project administration, Funding acquisition.

Declaration of competing interest

The authors declare that they have no known competing financial interests or personal relationships that could have appeared to influence the work reported in this paper.

Data availability

Data will be made available on request.

Acknowledgments

This work was supported by the High Luminosity Upgrade of LHC UK - Phase II, UK and the STFC Cockcroft core grant, UK.

References

[1] R. Anne, Y. Georget, R. Hue, C. Tribouillard, J. Luc Vignet, A noninterceptive heavy ion beam profile monitor based on residual gas ionization, Nucl. Instrum. Methods Phys. Res. A 329 (1) (1993) 21–28, http://dx.doi.org/10.1016/0168-9002(93)90918-8, URL https://www.sciencedirect.com/science/article/pii/0168900293909188.

[2] J. Mießner, M. Sachwitz, M. Markert, R. Sternberger, K. Tiedtke, A. Hofmann, An ionization profile monitor for the determination of the FLASH photon beam parameter, Nucl. Instrum. Methods Phys. Res. A 635 (1, Supplement) (2011) S104–S107, http://dx.doi.org/10.1016/j.nima.2010.10.155, URL https://www.sciencedirect.com/science/article/pii/S0168900210025039, PhotonDiag 2010.

[3] D. Bartkoski, C. Deibele, Y. Polsky, Design of an ionization profile monitor for the SNS accumulator ring, Nucl. Instrum. Methods Phys. Res. A 767 (2014) 379–384, http://dx.doi.org/10.1016/j.nima.2014.09.020.

[4] A. Variola, R. Jung, G. Ferioli, Characterization of a nondestructive beam profile monitor using luminescent emission, Phys. Rev. ST Accel. Beams 10 (2007) 122801, http://dx.doi.org/10.1103/PhysRevSTAB.10.122801, URL https://link.aps.org/doi/10.1103/PhysRevSTAB.10.122801.

[5] T. Tsang, D. Gassner, M. Minty, Residual gas fluorescence monitor for relativistic heavy ions at RHIC, Phys. Rev. ST Accel. Beams 16 (10) (2013) 102802, http://dx.doi.org/10.1103/PhysRevSTAB.16.102802.

[6] P. Forck, A. Bank, Residual gas fluorescence for profile measurements at the GSI UNILAC, in: Proc. EPAC'02, Paris, France, 2003, pp. 1885–1887, https://jacow.org/e02/papers/THPRI056.pdf.

[7] P. Forck, Minimal invasive beam profile monitors for high intense hadron beams, in: Proc. IPAC'10, Kyoto, Japan, 2010, pp. 1261–1265, http://accelconf.web.cern.ch/IPAC10/papers/TUZMH01.pdf.

[8] F. Becker, C. Andre, P. Forck, D. Hoffmann, Beam induced fluorescence (BIF) monitor for transverse profile determination of 5 to 750 MeV/u heavy ion beams, in: Proc. DIPAC'07, Venice, Italy, 2007, pp. 33–35, https://jacow.org/d07/papers/MOO3A02.pdf.

[9] Y. Hashimoto, T. Fujisawa, T. Morimoto, Y. Fujita, T. Honma, S. Muto, K. Noda, Y. Sato, S. Yamada, Oxygen gas-sheet beam profile monitor for the synchrotron and storage ring, Nucl. Instrum. Methods Phys. Res. A 527 (3) (2004) 289–300, http://dx.doi.org/10.1016/j.nima.2004.05.034, URL https://www.sciencedirect.com/science/article/pii/S0168900204009714.

[10] T. Fujisawa, Y. Hashimoto, T. Morimoto, Y. Fujita, Multi-pole magnets to focus an O2 sheet beam for a non-destructive beam-profile monitor, Nucl. Instrum. Methods Phys. Res. A 506 (1) (2003) 50–59, http://dx.doi.org/10.1016/S0168-9002(03)01393-7, URL https://www.sciencedirect.com/science/article/pii/S0168900203013937.

[11] V. Tzoganis, C.P. Welsch, A non-invasive beam profile monitor for charged particle beams, Appl. Phys. Lett. 104 (20) (2014) 204104, http://dx.doi.org/10.1063/1.4879285.

[12] V. Tzoganis, H.D. Zhang, A. Jeff, C.P. Welsch, Design and first operation of a supersonic gas jet based beam profile monitor, Phys. Rev. Accel. Beams 20 (2017) 062801, http://dx.doi.org/10.1103/PhysRevAccelBeams.20.062801, URL https://link.aps.org/doi/10.1103/PhysRevAccelBeams.20.062801.

[13] A. Salehilashkajani, H.D. Zhang, M. Ady, N. Chritin, P. Forck, J. Glutting, O.R. Jones, R. Kersevan, N. Kumar, T. Lefevre, et al., A gas curtain beam profile monitor using beam induced fluorescence for high intensity charged particle beams, Appl. Phys. Lett. 120 (17) (2022) 174101, http://dx.doi.org/10.1063/5.0085491.

[14] V. Tzoganis, A. Jeff, C.P. Welsch, Gas dynamics considerations in a non-invasive profile monitor for charged particle beams, Vacuum 109 (2014) 417–424, http://dx.doi.org/10.1016/j.vacuum.2014.07.009, URL https://www.sciencedirect.com/science/article/pii/S0042207X14002450.

[15] K. Zapfe, B. Braun, H. Gaul, M. Grieser, B. Povh, M. Rall, E. Steffens, F. Stock, J. Tonhäuser, C. Montag, F. Rathmann, D. Fick, W. Haeberli, High density polarized hydrogen gas target for storage rings, Rev. Sci. Instrum. 66 (1) (1995) 28–31, http://dx.doi.org/10.1063/1.1146388.

[16] A. Gruber, W. Bourgeois, B. Franzke, A. Kritzer, C. Treffert, Internal gas-jet target for the ESR at GSI, Nucl. Instrum. Methods Phys. Res. A 282 (1) (1989) 87–93, http://dx.doi.org/10.1016/0168-9002(89)90114-9, URL https://www.sciencedirect.com/science/article/pii/0168900289901149.

[17] F. Favela, L. Acosta, E. Andrade, V. Araujo, A. Huerta, O.G. de Lucio, G. Murillo, M.E. Ortiz, R. Policroniades, P. Santa Rita, A. Varela, E. Chávez, New supersonic gas jet target for low energy nuclear reaction studies, Phys. Rev. ST Accel. Beams 18 (2015) 123502, http://dx.doi.org/10.1103/PhysRevSTAB.18.123502, URL https://link.aps.org/doi/10.1103/PhysRevSTAB.18.123502.

[18] D. Shapira, J. Del Campo, J. Ford, B. Shivakumar, P. Stelson, B. Harmon, R. Parks, S. Thornton, Nuclear physics experiments with the ornl-hhirf supersonic gas jet target, Nucl. Instrum. Methods Phys. Res. B 10–11 (1985) 436–440, http://dx.doi.org/10.1016/0168-583X(85)90285-X, URL https://www.sciencedirect.com/science/article/pii/0168583X8590285X.

[19] A. Kontos, D. Schürmann, C. Akers, M. Couder, J. Görres, D. Robertson, E. Stech, R. Talwar, M. Wiescher, HIPPO: A supersonic helium jet gas target for nuclear astrophysics, Nucl. Instrum. Methods Phys. Res. A 664 (1) (2012) 272–281, http://dx.doi.org/10.1016/j.nima.2011.10.039, URL https://www.sciencedirect.com/science/article/pii/S0168900211019899.

[20] J. Ullrich, R. Moshammer, A. Dorn, R.D. rner, L.P.H. Schmidt, H.S.-B. cking, Recoil-ion and electron momentum spectroscopy: reaction-microscopes, Rep. Progr. Phys. 66 (9) (2003) 1463–1545, http://dx.doi.org/10.1088/0034-4885/66/9/203.

[21] K.Y. Kim, V. Kumarappan, H.M. Milchberg, Measurement of the average size and density of clusters in a gas jet, Appl. Phys. Lett. 83 (15) (2003) 3210–3212, http://dx.doi.org/10.1063/1.1618017.

[22] T. Ditmire, R.A. Smith, Short-pulse laser interferometric measurement of absolute gas densities from a cooled gas jet, Opt. Lett. 23 (8) (1998) 618–620, http://dx.doi.org/10.1364/OL.23.000618, URL http://ol.osa.org/abstract.cfm?URI=ol-23-8-618.

[23] B. Landgraf, M. Schnell, A. Sävert, M.C. Kaluza, C. Spielmann, High resolution 3D gas-jet characterization, Rev. Sci. Instrum. 82 (8) (2011) 083106, http://dx.doi.org/10.1063/1.3624694.

[24] X. Gao, X. Wang, B. Shim, A.V. Arefiev, R. Korzekwa, M.C. Downer, Characterization of cluster/monomer ratio in pulsed supersonic gas jets, Appl. Phys. Lett. 100 (6) (2012) 064101, http://dx.doi.org/10.1063/1.3683543.

[25] K. Schmid, L. Veisz, Supersonic gas jets for laser-plasma experiments, Rev. Sci. Instrum. 83 (5) (2012) 053304, http://dx.doi.org/10.1063/1.4719915.

[26] S. Lorenz, G. Grittani, E. Chacon-Golcher, C.M. Lazzarini, J. Limpouch, F. Nawaz, M. Nevrkla, L. Vilanova, T. Levato, Characterization of supersonic and subsonic gas targets for laser wakefield electron acceleration experiments, Matter Radiat. Extrem. 4 (1) (2019) 015401, http://dx.doi.org/10.1063/1.5081509.

[27] C. Stern, J. Alvarado, C. Aguilar, Density measurements in a supersonic jet, J. Mech. Mater. Struct. 2 (8) (2007) 1437–1448, http://dx.doi.org/10.2140/jomms.2007.2.1437.

[28] R. Rajeev, S.V. Raja, T. Madhu Trivikram, K.P.M. Rishad, M. Krishnamurthy, Measurement of the spatio-temporal gas density profile of a supersonic jet, J. Appl. Phys. 114 (8) (2013) 083112, http://dx.doi.org/10.1063/1.4819448.

[29] M. Patel, J. Thomas, H.C. Joshi, Flow characterization of supersonic gas jets: Experiments and simulations, Vacuum 192 (2021) 110440, http://dx.doi.org/10.1016/j.vacuum.2021.110440.

[30] N.E. Schofield, D.M. Paganin, A.I. Bishop, Absolute density-profile tomography of molecular beams using multiphoton ionization, Rev. Sci. Instrum. 80 (12) (2009) 123105, http://dx.doi.org/10.1063/1.3264079.

[31] C. Meng, M.H.M. Janssen, Measurement of the density profile of pure and seeded molecular beams by femtosecond ion imaging, Rev. Sci. Instrum. 86 (2) (2015) 023110, http://dx.doi.org/10.1063/1.4913251.

[32] J.G. Pronko, D. Kohler, I.V. Chapman, T.T. Bardin, P.C. Filbert, J.D. Hawley, Density measurements of a pulsed supersonic gas jet using nuclear scattering, Rev. Sci. Instrum. 64 (7) (1993) 1744–1747, http://dx.doi.org/10.1063/1.1144003.

[33] Y. Hashimoto, Y. Hori, T. Morimoto, T. Toyama, M. Uota, T. Fujisawa, T. Murakami, K. Noda, D. Ohsawa, Development of a beam profile monitor using a nitrogen-molecular jet for the J-PARC MR, in: Proc. IBIC'13, Oxford, UK, 2013, pp. 848–851, URL https://jacow.org/IBIC2013/papers/WEPF17.pdf.

[34] G. Scoles, Atomic and Molecular Beam Methods: Vol. 1, Oxford University Press, 1998, pp. 14–53, 272–275.

[35] H. Ashkenas, F.S. Sherman, Structure and utilization of supersonic free jets in low density wind tunnels, Tech. rep., No. NASA-CR-60423, 1965.

[36] J.B. Anderson, Inviscid freejet flow with low specific heat ratios., AIAA J. 10 (1) (1972) 112, http://dx.doi.org/10.2514/3.6551.

[37] A. Gruber, W. Bourgeois, B. Franzke, A. Kritzer, C. Treffert, Internal gas-jet target for the ESR at GSI, Nucl. Instrum. Methods Phys. Res. A 282 (1) (1989) 87–93, http://dx.doi.org/10.1016/0168-9002(89)90114-9, URL https://www.sciencedirect.com/science/article/pii/0168900289901149.

[38] P. Clausing, The flow of highly rarefied gases through tubes of arbitrary length, J. Vac. Sci. Technol. 8 (5) (1971) 636–646, http://dx.doi.org/10.1116/1.1316379.

[39] A. Salehilashkajani, et al., Non-invasive beam profile monitoring for the HL-LHC hollow electron lens, in: Proc. IPAC'21, Campinas, Brazil, 2021, pp. 884–887, http://dx.doi.org/10.18429/JACoW-IPAC2021-MOPAB279, URL https://jacow.org/ipac2021/papers/MOPAB279.pdf.

[40] N. Kumar, A. Salehilashkajani, H. Zhang, M. Ady, P. Forck, J. Glutting, O. Jones, R. Kersevan, T. Marriott-Doddington, S. Mazzoni, et al., Non-invasive beam profile monitor for medical accelerators, Phys. Medica 73 (2020) 173–178, http://dx.doi.org/10.1016/j.ejmp.2020.04.023.